www.czasopisma.pan.pl PAN POLSKA AKADEMIA NAUK www.journals.pan.pl

A R C H I V E S O F M E T A L L U R G Y A N D M A T E R I A L S

Volume 60 2015 Issue 2

DOI: 10.1515/amm-2015-0144

P. DHARMAIAH*, H.-S. KIM*, K.-H. LEE**, S.-J. HONG*,♯

FABRICATION OF Zn_4Sb_3 ALLOYS BY A COMBINATION OF GAS-ATOMIZATION AND SPARK PLASMA SINTERING PROCESSES

WYTWARZANIE I KONSOLIDACJA PROSZKÓW STOPOWYCH Zn_4Sb_3 PRZEZ KOMBINACJĘ PROCESÓW ATOMIZACJI GAZOWEJ I SPIEKANIA

In this study, single phase polycrystalline Zn_4Sb_3 as well as 11 at.% Zn-rich Zn_4Sb_3 alloy having ε-Zn_4Sb_3 (majority phase) and Zn (minority phase) phases bulk samples produced by gas-atomization and subsequently consolidated by spark plasma sintering (SPS) process. The crystal structures were analyzed by X-ray diffraction (XRD) and cross-sectional microstructure were observed by the scanning electron microscopy (SEM). The internal grain microstructure of 11at.% Zn-rich Zn_4Sb_3 powders shows lamellar structure. Relative density, Vickers hardness and crack lengths were measured to investigate the effect of sintering temperature of Zn_4Sb_3 samples which are sintered at 653, 673 and 693 K. Relative density of the single phase bulk Zn_4Sb_3 sample reached to 99.2% of its theoretical density. The micro Vickers hardness of three different sintering temperatures were found around 2.17 – 2.236 GPa.

Keywords: Gas atomization, Microstructure, Spark plasma sintering (SPS), X-ray diffraction

1. Introduction

Thermoelectric materials have been fascinated extensive interest due to increasing demand for cooling devices and reuse of waste heat convert into electrical energy for power generation applications.Well established thermoelectric materials used in thermoelectric devices can be divided into three types depending upon their temperature range of applications. Bi_2Te_3 and its alloys work around temperature range 300-500 K. In the intermediate temperature range 600-900 K, PbTe-based alloys and TAGS (Te-Ag-Ge-Sb) are the most efficient materials. At the high temperature range (1000-1300 K), Si-Ge alloys are mainly used in power generation devices for space applications. PbTe based alloys are toxic and it has significant adverse impacts on human health and eco-environment issue. However, alternative materials are urgently needed to replace PbTe alloys. Among the thermoelectric materials p-type semiconductive β-Zn_4Sb_3 compound as a new material with high figure of merit ZT= 1.3 in the 300-670 K temperature range have identified by Caillat et al. [1]. ZT value can be increased by increasing Seebeck coefficient and electrical conductivity, or decreasing its thermal conductivity. However, these parameters are not independent, because the thermal conductivity (k) is the sum of the lattice thermal conductivity (k_L) and electrical contribution (k_e) which is strongly depends on the electrical conductivity by Wiedemann-Franz law. In order to increase ZT, the most powerful technique is to lower the lattice thermal conductivity while maintaining good electrical transport properties.

For Zn_4Sb_3 has three modifications: α, β and γ phases which are stable below 263 K, between 263 and 765 K, and above 765 K, respectively. The phase diagram investigated by Mayer et al. [2] β- Zn_4Sb_3 has a hexagonal rhombohedric crystal structure, space group R3C with a= 12.231Å and c= 12.428 Å [2,3]. Due to this reason, the fabrication of single-phase Zn_4Sb_3 samples involves complicated process [1, 4, 5]. Low thermal conductivity values can be expected because of its complex structure. Caillat et al. reported a room temperature thermal conductivity value around 0.9 Wm^{-1} K^{-1}, which was lower than that of a state of the art of Bi_2Te_3, based thermoelectric materials [6].

Several fabrication methods for Zn_4Sb_3 have been introduced, such as mechanical alloying (MA) [7, 8], vacuum melting process [9], bulk mechanical alloying (BMA) followed by hot pressing [10], melting in an evacuated quartz ampoule followed by a granulation and hot consolidation process [1, 3]. To best of our knowledge, no one can report Zn_4Sb_3 alloys by using gas atomization and spark plasma sintering process. Among all of the above, gas-atomization is more attractive due to its efficient and high performance applications. It is useful for mass production of thermoelectric materials, easy process control, requires short duration of time and homogeneous pro-

* DIVISION OF ADVANCED MATERIALS ENGINEERING, KONGJU NATIONAL UNIVERSITY, CHEONAN CITY REPUBLIC OF KOREA

** DEPARTMENT OF NANO MATERIALS ENGINEERING, CHUNGNAM NATIONAL UNIVERSITY, DAEJEON 305-764, KOREA

♯ Corresponding author: hongsj@kongju.ac.kr

ductivity without isolation relative to other fabrication process [11-13].

In this study, we have been fabricated single phase Zn_4Sb_3 based alloys by a combination of gas-atomization and SPS process. The morphology, microstructure and mechanical properties including Vickers hardness, crack length with different consolidation temperatures were evaluated and discussed.

Also, Zn-rich Zn_4Sb_3) alloy powder was prepared by GA(same conditions with previous) and consolidated by SPS at 723 K, and then analyzed their properties.

2. Experimental procedure

High-purity antimony granules (99.999%) and zinc bars (99.999%) were used as raw materials in this study. The raw elements were weighed for the required stoichiometric ratio, and nominally 11 at.% Zn-rich mixture to compensate for possible Zn loss during melting. The alloy was melted at 500°C above the liquidus temperature under Ar atmosphere to make the master alloy, and then bottom pouring the melt through a boron nitride melt delivery nozzle of 8 mm diameter to a N_2 gas operated atomizer working at a pressure of 1.2 MPa, the rapidly solidified powders were produced [11, 12]. The size distribution of the as-atomized powders was carried out by laser diffraction technique using Mastersizer 2000 particle analyzer. The Zn_4Sb_3 powders were consolidated at 653 K, 673 K, 693 K, and 11 at.% Zn-rich Zn_4Sb_3 (named as Zn-rich Zn_4Sb_3) powders consolidated at 723 K by using spark plasma sintering under a pressure of 50 MPa in a diameter of 20 mm graphite mould in vacuum for 10 min. Relative densities of the samples were measured by the Archimedes method. Phase identification of the as-atomized powders and sintered bulks were performed by X-ray diffractometer (Rigaku, MiniFlex-600, Japan) using high energy monochromatic CuKα radiation (15.418 nm) in the 2θ range from 20 to 60 degrees at a scan rate of 0.02°/s. The morphology and cross-sectional microstructure of the powders were observed by the scanning electron microscopy (SEM-MIRA LMH II (TESKAN), USA) after polishing and etching by a solution of HNO_3 and H_2O in the ratio of 1:1 for 3 min. Vickers hardness was measured by indentation of a diamond pyramid on the polished surface of the samples with Vickers hardness tester. The load applied during the hardness test was 500 gf with dwell time being 15s. For accuracy, 20 to 25 indentations were carried out for each sample and then averaged. The cracks were generated at the corners of indentations during the Vickers hardness testing and measured by using SEM micrographs.

3. Results and discussion

Fig.1 shows the XRD patterns of the starting powders and sintered bulks of Zn_4Sb_3, and Zn-rich Zn_4Sb_3 respectively, obtained from gas atomization and spark plasma sintering. The XRD spectra were compared and indexed with Joint Committee on Powder Diffraction Standards (JCPDS) database PDF Nos.341013 and 400809 for Zn_4Sb_3 and ZnSb phases respectively [14]. The X-ray diffraction pattern of the starting powder phases are identified as ε-Zn_4Sb_3 and β-ZnSb. It is known that, the possible reason of β-ZnSb phase is due to partial decomposition of Zn_4Sb_3 and corresponding Zn loss at temperatures over 523 K under dynamic vacuum [15]. The sintered Zn_4Sb_3 samples at 653 K under pressure of 50 MPa exhibit the single ε-Zn_4Sb_3 phase, where as Zn-rich Zn_4Sb_3 SPSed samples at 723 K under pressure of 50 MPa identified as excess Zn phase because of adding excess Zn. If it is correct assumption the evaporation of Zn, β-ZnSb phase should remain after sintering process. But, the β-ZnSb phase does not observed in sintered samples. From the above discussion, we conclude that the β-ZnSb phase in the starting powders is not due to decomposition of Zn_4Sb_3 but it may be due to incomplete solidification of Zn and Sb in the gas atomization process. Single-phase Zn_4Sb_3 with 99.24% of its theoretical density was successfully produced at 653 K as shown in Fig. 1(c) and Table. 1.

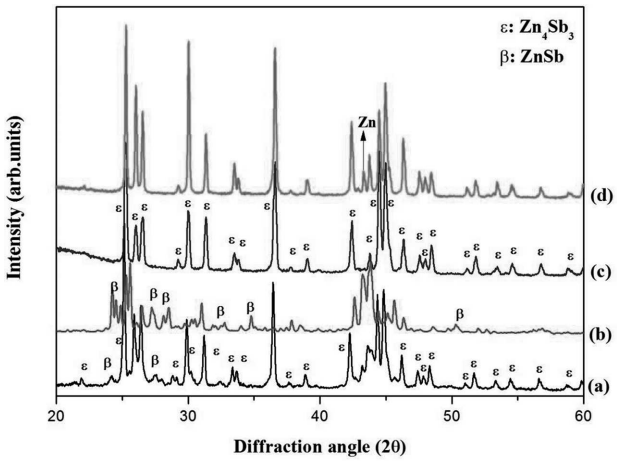

Fig. 1. X-ray diffraction patterns of (a) stoichiometric powder (b) over stoichiometric powder (Zn-rich) (c) SPSed bulks of stoichiometric powder at 653 K, (d) SPSed bulks of over stoichiometric powder at 723 K

TABLE 1
Mechanical properties of Zn_4Sb_3 and Zn-rich Zn_4Sb_3 spark plasma sintered bulks under various temperatures

Sample	SPS temperature (K)	Bulk density (gcm^{-3})	Relative density (%)
Zn_4Sb_3	653	6.3220	99.24
Zn_4Sb_3	673	6.3302	99.37
Zn_4Sb_3	693	6.3379	99.49
Zn+Zn_4Sb_3	723	6.3394	99.52

* Adopted theoretical density of 6.37 gcm^{-3} in ref. [16].

The log normal size distribution of gas-atomized stoichiometric Zn_4Sb_3, and Zn-rich Zn_4Sb_3 powders are shown in Fig. 2(a) and (b). The surface weighted mean and volume weighted mean of Zn_4Sb_3, and zinc-rich Zn_4Sb_3 powder particles are 21 μm, 54 μm and 13 μm, 44 μm respectively. The broad size distribution of Zn_4Sb_3 is shown in Fig. 2(a) specifies $D_{0.1}$ = 9.166 μm, $D_{0.5}$ = 35.991 μm and $D_{0.9}$ =130.121 μm corresponding to the particle sizes at 0.1, 0.5, and 0.9 volume

percentages respectively. A broad and bimodal size distribution of Zn-rich Zn_4Sb_3 powders could be indentified in Fig. 2(b) specifies $D_{0.1}$ = 5.460 μm, $D_{0.5}$ = 20.413 μm, and $D_{0.9}$ = 102.576 μm corresponding to the particle sizes at 0.1, 0.5, and 0.9 volume percentages respectively. Usually, gas atomization process results fairly wide range of particle size distribution due to the variation in the cooling rate, which is inversely proportional to the size of the liquid droplets [11]. Based on the results particle size distribution of Zn-rich Zn_4Sb_3 powders has narrower compared to Zn_4Sb_3 size distribution. However, thermoelectric and mechanical properties of the bulk alloys indirectly depend on the particle size which will affected to microstructure. For that reason many researchers concentrate on process parameters of gas atomization for producing fine particle sizes.

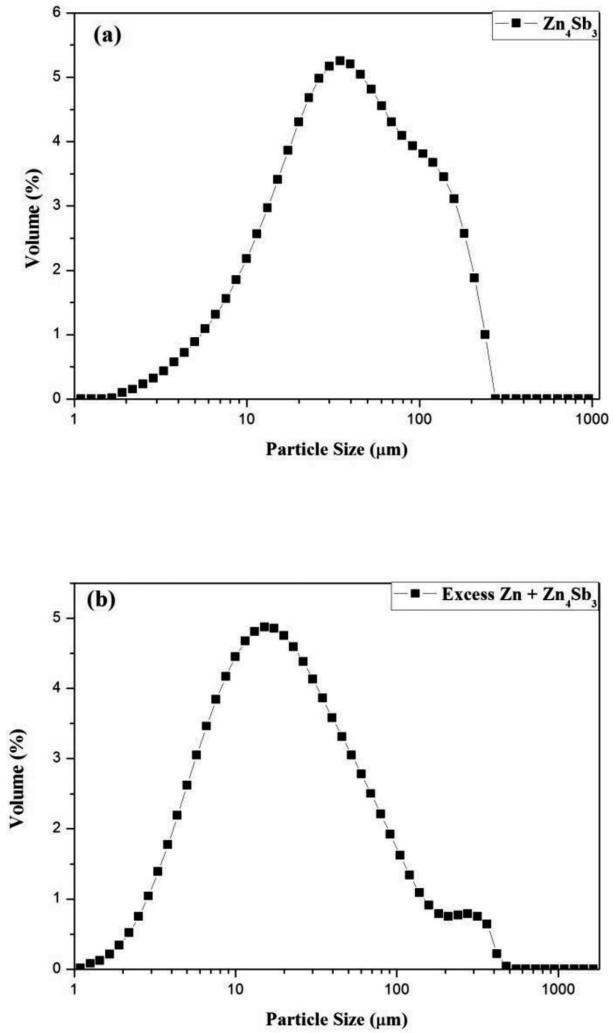

Fig. 2. Log normal size distributions of gas-atomized Zn_4Sb_3 powder (a) stoichiometric and (b) over stoichiometric (Zn-rich)

Fig. 3 shows a typical morphology and microstructure of Zn_4Sb_3, and Zn-rich Zn_4Sb_3 as atomized powders. Fig. 3(a, b) & (c, d) shows a low and high magnification morphology of as atomized powders. It is visible that all powder particles were spherical in shape. At high magnification as atomized powders have few satellites attached on the main powders. These satellites contribute to higher packing density and free flowing characteristics. The average diameter of the as-atomized Zn_4Sb_3, and Zn-rich Zn_4Sb_3 powder particles are around 30 μm and 20 μm, respectively. Fig. 3 (e) & (f) comparison of the internal microstructures for Zn_4Sb_3 and Zn-rich Zn_4Sb_3 atomized powders. As can be seen from Fig. 3(e) it appears, homogeneous and unevenly distributed irregular shaped grains were observed. The width of the grains was around 2-25 μm. Interestingly, the microstructure of Zn-rich Zn_4Sb_3 powder is different compared to Zn_4Sb_3 microstructure is shown in Fig. 3(f). The grain internal structure of Zn-rich Zn_4Sb_3 is lamellar structure. It seems that both powders have unevenly distributed irregular shaped grains, although the internal structures of grains are different. In gas-atomization process the grain size of the powders significantly decreased due to rapid solidification. It can be noticed that controlling of the grain size is one of the key parameter to enhance the thermoelectric properties. Physical and mechanical properties of specimens presented in Table. 1. It can be clearly seen from the Table. 1 calculated relative density increases as the sintering temperature increases from 653 K to 693 K at 50 MPa pressure. It is mainly due to the decrease of fractional porosity of the bulks with sintering temperature [17].

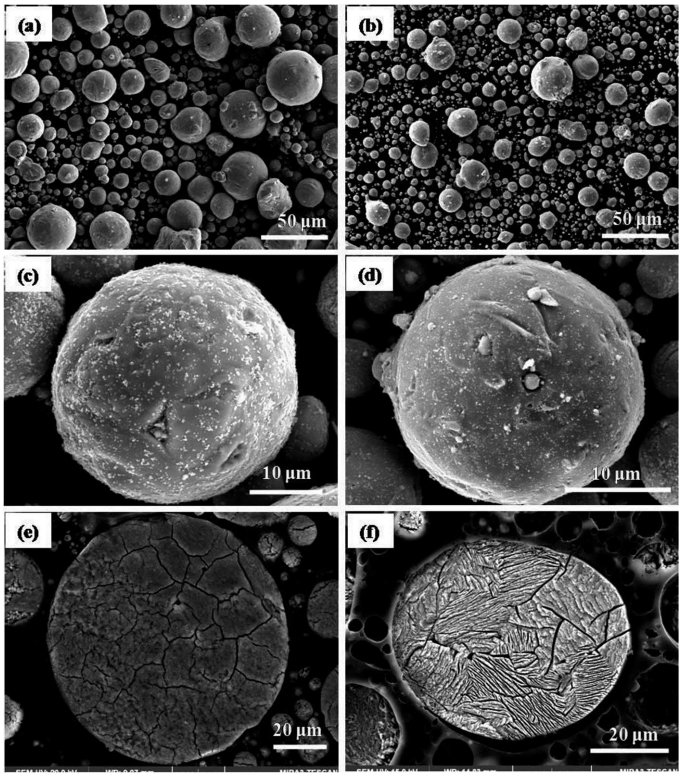

Fig. 3. SEM images of typical morphology (a & c), (b & d) low and high magnification of Zn_4Sb_3 and Zn-rich Zn_4Sb_3 as-atomized powders respectively, (e), (f) shows their corresponding microstructure

Fig. 4 shows the variation of Vickers hardness and Vickers indentation crack length with different consolidation temperatures. The Vickers hardness value increases with increasing sintering temperatures. The hardness of Zn_4Sb_3 samples uniform and stable ranging from 2.17 to 2.24 GPa. From these results, with higher sintering temperature guided to strong bonding in the Zn_4Sb_3 lattice and fewer crystal defects. Vickers hardness of Zn-rich Zn_4Sb_3 alloy is 2.1 GPa. The Vickers hardness values of Zn_4Sb_3, and Zn-rich Zn_4Sb_3 alloys comparable to other reported papers [18]. The Vickers hardness

value decreases with the addition of excess Zn to the Zn_4Sb_3 alloys. However, it may expect that high hardness of Zn_4Sb_3 bulks would considerably decrease material wastage during cutting process of the module. Hence, gas-atomized powders might posses good mechanical properties. Unfortunately, a large number of macroscopic cracks were observed in Zn_4Sb_3 alloys. It should be noticed that all sintered bulks were brittle and broke while cutting before the thermoelectric properties measurements. We realize that, it is difficult to produce crack free samples of Zn_4Sb_3 alloys by using combination of gas-atomization and spark plasma sintering process. It can be seen in Fig. 4 the crack length increases gradually and decreases at various sintering temperatures. The propagation of crack lengths are essential translates into high fracture toughness and high hardness values at a time. Crack length also one of the key parameter for fracture toughness. The crack length of Zn-rich Zn_4Sb_3 sample has low compared to Zn_4Sb_3 specimen at 673 K. This might be due to fine grain size of Zn-rich Zn_4Sb_3 specimen compared to Zn_4Sb_3 grains.

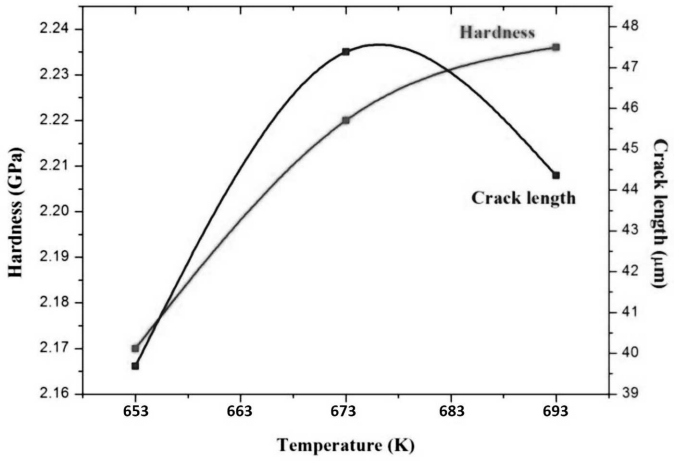

Fig. 4. The variation of Vickers hardness and Vickers indentation crack lengths of ε-Zn_4Sb_3 SPSed specimens at various sintering temperatures

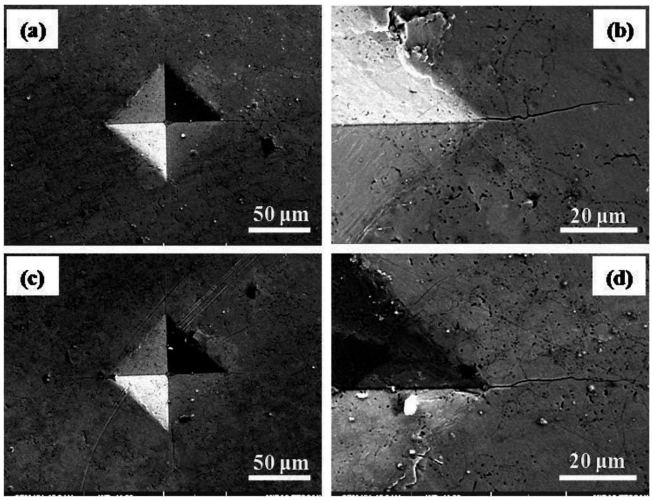

Fig. 5. SEM micrographs of indentation cracks generating from the edges. (a, b) low and high magnification image of Zn_4Sb_3, (c, d) low and high magnification image of Zn-rich Zn_4Sb_3

Fig. 5 shows SEM micrographs of Vickers indentation on polished surface of (a) Zn_4Sb_3 and, (b) Zn-rich Zn_4Sb_3 sample. Obviously, four cracks are extending from the corners of pyramidal indentation are seen in Zn_4Sb_3 samples. The crack positions of different sintered temperature of Zn_4Sb_3 samples are observed at corner. The four cracks enlarging from corners as well as one crack observed from circumference of the Vickers indenter in Zn-rich Zn_4Sb_3 sample. The formation of circumference cracks evidence of high ductile nature of the materials [18].

4. Conclusions

Single phase of Zn_4Sb_3 bulk specimens with more than 99% of its theoretical density were successfully fabricated by gas atomization and spark plasma sintering process. Zn-rich Zn_4Sb_3 sample having ε-Zn_4Sb_3 (majority phase) and Zn (minority phase) phases were identified. Internal microstructure of as-atomized Zn-rich Zn_4Sb_3 powder has lamellar structure, which is not identified in stoichiometric powder of Zn_4Sb_3. The Vickers hardness increases gradually with increase in sintering temperature due to increasing of its relative density. The maximum Vickers hardness was found as 2.24 GPa at 693 K. The indentation crack positions of different sintered temperature of Zn_4Sb_3 samples are observed at corner. The four cracks enlarging from corners as well as one crack observed from circumference of the Vickers indenter in Zn-rich Zn_4Sb_3 sample due to high ductile nature of the materials. The combination of gas-atomization and spark plasma sintering process posses good mechanical properties due to high compatibility of the powders during rapid solidification.

Acknowledgements

This research was supported by Basic Science Research Program through the National Research Foundation of Korea (NRF) funded by the Ministry of Education, Science and Technology (2012R1A1A2008113).

REFERENCES

[1] T. Caillat, J.P. Fleurial, A. Borshchevsky, J. Phys. Chem. Solids. **58**, 1119 (1997).
[2] H.W. Mayer, I. Mikhali, K. Schubert, J. Less Comm. Met. **59**, 43 (1978).
[3] M. Tapiero, S. Tarabichi, J.G. Gies, C. Noguet, J.P. Zielinger, M. Joucla, J. Loison, M. Robino, J. Henrion, Sol. Energy Mater. **12**, 257 (1985).
[4] V. Izard, M.C. Record, J.C. Tedenac, S.G. Fries, Calphad. **25**, 567 (2001).
[5] S. Ur, P. Nash, I. Kim, J. Alloys Compd. **361**, 84 (2003).
[6] K.T. Kim, K.M. Jang, K.J. Kim, G.H. Ha, J. Kor. Powd. Met. Inst. **17**, 2 (2010).
[7] E.K. Park, S.M. Hong, J.J. Park, M.K. Lee, C.K. Rhee, K.W. Seol, J. Kor. Powd. Met. Inst. **20**, 4 (2013).
[8] V. Izard, M.C. Record, J.C. Tedenac, J. Alloys Compd. **345** , 257 (2002).
[9] T.J. Zhu, X.B. Zhao, M. Yan, S.H. Hu, T. Li, B.C. Chou, Mater. Lett. **46**, 44 (2000).
[10] T. Aizawa, Y. Iwaisako, K.I. Fukagawa, A. Yamamoto, in: Proceedings of the 18th international conference on thermoelectrics **173**, USA (1999).

[11] M.H. Bhuiyan, T.S. Kim, J.M. Koo, S.J. Hong, J. Alloys Compd. **509**, 1722 (2011).
[12] S.J. Hong, S.H. Lee, B.S. Chun, Mater.Sci.Eng. B. **98**, 232 (2003).
[13] S.J. Hong, B.S. Chun, Mater. Res. Bull. **38**, 599 (2003).
[14] Powder Diffract. File, JCPDS-ICDD, 12 Campus Boulevard, Newtown Square, PA 19073, USA (2001).
[15] T. Caillat, J. Fleurial, A. Borshchevsk, in: Proceedings of the 15th international conference on thermoelectrics, Pasadena, 151, USA (1996).
[16] G.J. Snyder, M. Christensen, E. Nishibori, T. Caillat, B.B. Iversen, Nat. Mater. **3**, 458 (2004).
[17] J.H. Ahn, M.W. Oh, B.S. Kim, S.D. Park, B.K. Min, H.W. Lee, Y.J. Shim, Mater. Res. Bull. **46**, 1490 (2011).
[18] S. Ur, P. Nash, R. Schwarz, Met. Mater. Int. **11**, 435 (2005).

Received: 20 November 2014.